Hyperspectral imaging in the digitisation of museum artefacts: technical aspects, initial processing and methods for data analysis and visualisation

DOI: 10.5604/01.3001.0055.1371

***Paulina Krupska-Wolas*[1, 2], *Michał Obarzanowski*[1], *Tomasz Wilkosz*[1], *Julio M. del Hoyo-Meléndez*[1]**

[1] *Laboratory of Analysis and Nondestructive Investigation of Heritage Objects*
National Museum in Cracow
[2] *Faculty of Physics and Applied Computer Science*
AGH University of Science and Technology in Cracow

Wilanów Studies
vol. XXXI, 2024, pp. 199–244
Yearbook, E-ISSN: 2720-0116

Preface

In the field of cultural heritage research, non-invasive surveys play a key role due to the extent of information they can provide about the artefact without impacting its integrity. Imaging techniques are particularly important in this field due to the fact that they provide a global view of the artefact, enabling the experts to appreciate certain features in relation to the complete work and the artist's craftsmanship.

Full-spectrum electromagnetic photography is a very popular tool used for digitalising museum artefacts and studying the collections in the broadest sense of the concept, with the aim to assess their state of preservation, material composition, design, and the application of conservation strategies and treatments.

In addition to conventional analytical photography, spectroscopic imaging systems are becoming increasingly popular. There are several categories of such solutions, which encompass imaging devices using elemental analysis (e.g. XRF,[1] scanning electron microscopy[2]) and molecular analysis (using visible and infrared light reflections,[3] X-ray diffraction,[4] the Raman effect[5] and other techniques). In order to provide a comprehensive description of an object, experts often resort to using a number of complementary techniques.[6]

1 M. Alfeld et al., 'A mobile instrument for in situ scanning macro-XRF investigation of historical paintings', *Journal of Analytical Atomic Spectrometry*, vol. 28(5), 2013, pp. 760–767.

2 C. J. G. van Hoek et al., 'A SEM-EDS Study of Cultural Heritage Objects with Interpretation of Constituents and Their Distribution Using PARC Data Analysis', *Microscopy and Microanalysis*, vol. 17(5), 2011, pp. 656–660.

3 J. K. Delaney et al., 'Visible and infrared imaging spectroscopy of paintings and improved reflectography', *Heritage Science*, vol. 4(6), 2016.

4 V. Gonzales et al., 'X-ray Diffraction Mapping for Cultural Heritage Science: a Review of Experimental Configurations and Applications', *Chemistry. A European Journal*, vol. 26(8), 2019.

5 A. Rousaki, P. Vandenabeele, 'In situ Raman spectroscopy for cultural heritage studies', *Journal of Raman Spectroscopy*, vol. 52, 2021.

6 E. Catelli et al., 'Towards the non-destructive analysis of multilayered samples: A novel XRF-VNIR-SWIR hyperspectral imaging system combined with multiblock data processing', *Analytica Chimica Acta*, vol. 1239, 2023; J. K. Delaney et al., 'Integrated X-ray fluorescence and diffuse visible-to-near-infrared reflectance scanner for standoff elemental and molecular spectroscopic imaging of paints and works on paper', *Heritage Science*, vol. 6(31), 2018; L. M. Smieska et al., 'Synchrotron-Based High-Energy X-ray MA-XRF and MA-XRD for Art and Archaeology', *Synchrotron Radiation News*, vol. 32(6), 2019.

In order to understand the possibilities offered by imaging techniques as far as works of art are concerned, one needs to start by understanding the phenomena that underpin the creation of the images, which are captured by the cameras used for studying historic artefacts.

This paper focuses on multiband imaging techniques (selected conventional analytical photography techniques), as well as (multi)hyperspectral imaging techniques: reflectance spectroscopy imaging in the visible (Vis), near infrared (NIR) and the short-wavelength infrared (SWIR), in the context of the digitalisation of museum artefacts.

Light and matter interactions

The images captured by cameras are the result of the interaction of the light source's radiation with the object's matter. Each photon that is part of the light stream generated by the light source can be absorbed, reflected or scattered when it encounters an obstacle (including the observed object). The energy of the photons emitted by a standard lamp is measured in electron volts (eV) and can cause electron and oscillatory excitations in the molecular structure of the object's material.

Matter is made up of molecules made up of atoms joined together by chemical bonds. Each molecule holds several types of energy – kinetic energy (not applicable to static objects), rotational energy (the spinning of atoms and molecules around their own axis), oscillatory energy (the change in the length and angles of bonds between the atoms of a molecule), electron energy (the energy levels of electrons) and the spin energy of the nuclei of atoms. The absorption of a photon with an energy measured in eV can excite a molecule by changing its oscillatory and electron energies. The excited particle strives to reach the ground state through de-excitation. These methods are shown on a diagram developed by Jabłoński.[7]

Each molecule is only able to absorb those photons with an energy corresponding to the energy difference in its oscillation or electron levels. De-excitation stands for a number of processes, including oscillatory relaxation, as well as fluorescence or phosphorescence. As a result of these processes, the detectors of the instruments are able to capture the backscattered photons. These photons have energies characteristic of the de-excitation process in a particular molecule, which directly translate into wavelength (according to the $E = \frac{hc}{\lambda}$ formula, where E is the energy, h is Planck's constant, c is the speed of light, and λ is the wavelength).

In view of the above, the image obtained from the measurement (in reflection mode) is the sum of all the relaxation processes of the photographed

7 A. Jablonski, 'Efficiency of Anti-Stokes Fluorescence in Dyes', *Nature*, vol. 131, 1933, pp. 839–840; J. R. Lakowicz, *Principles of Fluorescence Spectroscopy. Third edition*, 2006.

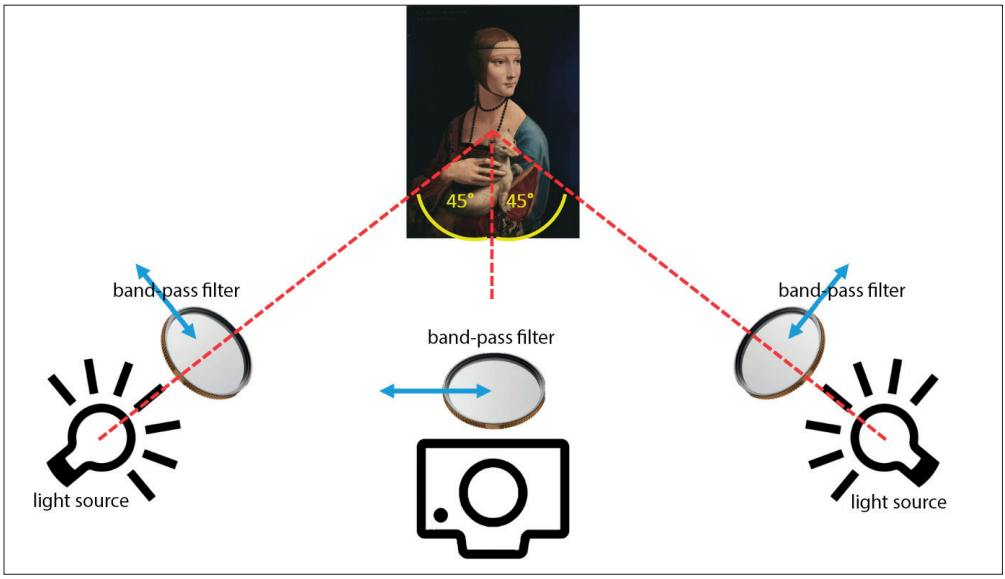

Fig. 1

Diagram of a test bed for multiband and (multi) hyperspectral imaging in the reflection mode

object and its surroundings excited by the source radiation. In her paper, Jana Striova summarised the phenomena that can be observed in the form of specific bands in the obtained reflectance spectra in relation to the molecular structure of the analysed material, in particular the pigments used.[8] It should also be kept in mind that many physical factors, among them the roughness of the object's surface, size and density of the pigment grains in the binder, or the binder itself, also affect the final resulting image.

Broadband electromagnetic imaging systems

Images are captured by detecting radiation of a desired character (i.e. reflected, transmitted or induced) in a given spectral band of any width, by using appropriate spectral filters or dispersive optics. Depending on the type of light source or filter used, which allows an object to be illuminated with radiation in a selected spectral band (UV, Vis), a specific response of the material of the object under examination can be expected and a suitable measuring device can be provided. Figure 1 shows a diagram of a measurement station used for capturing multiband and (multi)hyperspectral images. As shown, the light source should be angled at 45° to avoid specular reflections from the object.[9] Depending on the lighting used and the desired resulting image, the positioning and type of band-pass filters used (indicated by blue arrows) can be freely modified. Filters in the object-to-camera path can also be replaced by

8 J. Striova et al., 'Reflectance imaging spectroscopy in heritage science', *La Rivista del Nuovo Cimento*, vol. 43, 2020, pp. 515–566.

9 International Commission on Illumination, *Technical Report. Colorimetry*, 2004.

a suitable optical system equipped with dispersive elements and readout electronics adapted to this kind of process.

The types of light sources and filters used along the path between the light source and the object and between the object and the capturing device can be adjusted in order to produce images with the relevant characteristics, for example images in visible light, IR, UV or UV-induced visible light. As far as the layout of the test bed and pre-processing of the resulting images are concerned, the recommended source is the guide to multispectral imaging published by the British Museum.[10]

It should also be noted that multiband and (multi)hyperspectral images can be acquired by scanning the object: point-by-point (whiskbroom imaging), line-by-line along a selected plane (pushbroom imaging) and by capturing the entire area,[11] where the entire frame area is captured in a given band using appropriate tuning filters.[12] In the case of whiskbroom and pushbroom imaging, wavelength-dependent intensity information is obtained through the use of optical systems equipped with dispersive elements and prisms.[13] Area-based imaging systems, are usually equipped with circular filters – LCTFs (Liquid Crystal Tunable Filter) and AOTFs (Acousto-Optic Tunable Filter).[14]

Image pre-processing

The resulting images should be adjusted to account for the intrinsic noise of the camera's sensor and the non-uniform illumination of the imaged

10 J. Dyer, G. Verri, J. Cupitt, *Multispectral Imaging in Reflectance and Photo-induced Luminescence modes. A User Manual*, 2013, researchgate.net/publication/267266175_Multispectral_Imaging_in_Reflectance_and_Photo-induced_Luminescence_modes_A_User_Manual (accessed 20 May 2024).

11 R. Pillay, J. Y. Hardeberg, S. George, 'Hyperspectral Calibration of Art: Acquisition and Calibration Workflows', *Journal of the American Institute of Conservation*, vol. 58(1), 2019; M. Picollo et al., 'Hyper-Spectral Imaging Technique in the Cultural Heritage Field. New Possible Scenarios', *Sensors*, vol. 20(10), 2020; Q. Li et al., 'Review of spectral imaging technology in biomedical engineering. Achievements and challenges', *Journal of Biomedical Optics*, vol. 18, 2013.

12 Li et al., 'Review of spectral imaging technology'; N. Hagen et al., 'Snapshot advantage: A review of the light collection improvement for parallel high-dimensional measurement systems', *Optical Engineering*, vol. 51, 2012, pp. 1–7; O. Pust, 'Innovative Filter Solutions for Hyperspectral Imaging', *Optik & Photonik*, vol. 11(3), 2016.

13 R. Pillay, J. Y. Hardeberg, S. George, 'Hyperspectral Calibration of Art'; M. Picollo et al., 'Hyper-Spectral Imaging Technique'.

14 Li et al., 'Review of spectral imaging technology'; Hagen et al., 'Snapshot advantage'; Pust, 'Innovative Filter Solutions'; H. Lee, M. H. Kim, 'Building a Two-Way Hyperspectral Imaging System with Liquid Crystal Tunable Filters', in: *Image and Signal Processing, 6th International Conference, ICISP 2014*, vol. 8509, 2014, (Lecture Notes in Computer Science); R. Abdlaty, Q. Fang, 'Acousto-optic tunable filter-based hyperspectral imaging system characterization, SPIE BiOS 2019', *Design and Quality for Biomedical Technologies XII*, 2019.

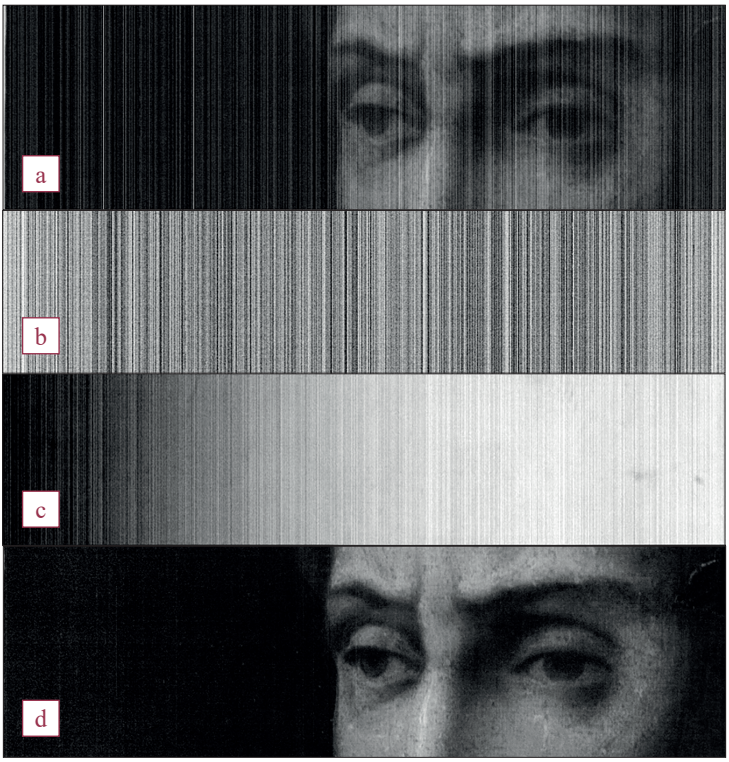

Fig. 2a–d

A selected frame from the painting *A Portrait of Dante* by an anonymous painter, held by the National Museum in Cracow: (a) fragment of the raw image without pre-processing; (b) dark current image; (c) white field image; (d) resulting processed image; in the case of images in the visible light spectrum, an additional correction against a colour test target (e.g. ColorChecker) needs to be carried out[16] to ensure proper colour reproduction

object, which can result from both imperfections in the geometry of the measurement system and the spatial structure of the object itself.

The correction of the noise generated by the sensor electronics when the aperture is closed (i.e. when no radiation is recorded), is performed by subtracting the dark current from the photograph of the object. This process eliminates the offset – non-zero sensor base values.

The next step is flat-field correction, which accounts for the differences in the spatial response of the sensor and takes into account the inconsistencies of the lighting. Thanks to the process, each pixel exhibits a consistent response to a given level of excitation. This correction entails dividing the image after noise cancelling by the image of the white field (which also requires noise compensation). If the photographed white field is not identical to the white benchmark, the brightness values of both images must be normalised to the same value.

All images – of the object, noise and white field – should be captured using the same parameters. An example of noise compensation and flat field correction is presented below.[15]

15 J. Dyer, G. Verri, J. Cupitt, *Multispectral Imaging*; R. Pillay, J. Y. Hardeberg, S. George, 'Hyperspectral Calibration of Art'; C. Jones et al., 'Understanding Multispectral Imaging of Cultural Heritage. Determining Best Practice in MSI Analysis of Historical Artefacts', *Journal of Cultural Heritage*, vol. 45(1), 2020.

16 H. Lee, *Introduction to Color Imaging Science*, New York 2005.

Multiband and multispectral imaging

Multiband imaging, or MBI for short, as well as multispectral imaging and hyperspectral imaging (MSI/HSI) are broad-spectrum imaging techniques. However, multiband imaging is not subject to spectral calibration and, as a result, the resulting data does not include spectra, which is not the case with multispectral imaging. The issue of calibrating multispectral and hyperspectral images is described in the 'Radiometric calibration and obtaining a spectrum' section of this paper.

For multiband imaging, the spectral bands remain relatively wide (>=100 nm). For example, visible-light photography is an example of multiband imaging (see fig. 3a), where the resulting image is a composite of three captured images, reflecting the red (600–800 nm), green (500–600 nm) and blue (400–500 nm) bands, respectively. The same applies to IR, UV or UV-induced Vis bands.

In order to obtain multispectral and hyperspectral images, they must undergo radiometric normalisation, whereby the pixel brightness reflects the reflectance level (see fig. 3b). The resulting set of photographs enables plotting a reflectance spectrum for each point in the image. Multispectral imaging happens when several or dozens of

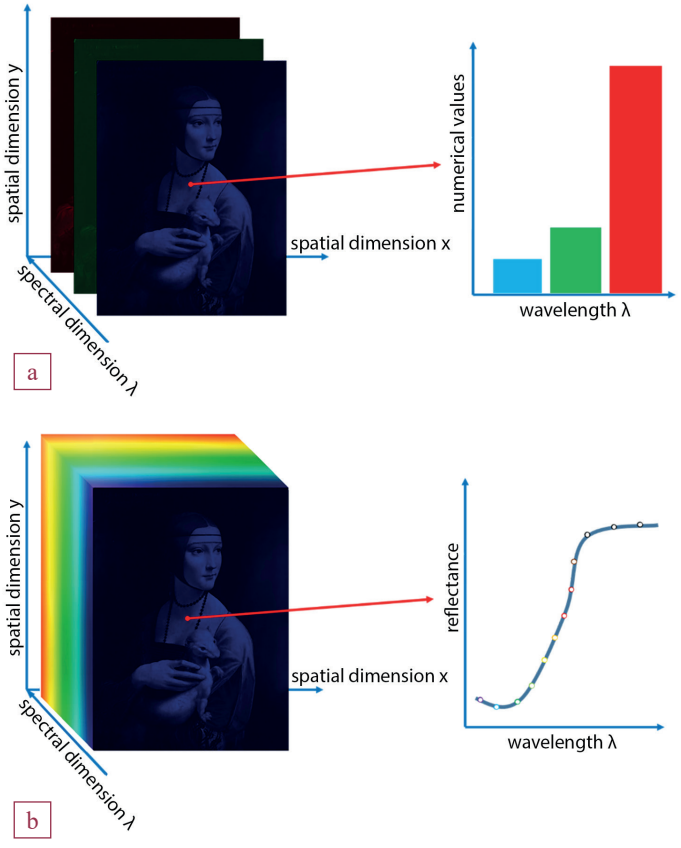

Fig. 3a–b

Conceptual representation of (a) multiband and (b) (multi) hyperspectral images

images capturing the broad range of the electromagnetic spectrum are considered. Hyperspectral images comprise a set of more than 100 images, with each shot capturing a narrow spectral range (often less than 1 nm), so that the resulting spectra appear to be continuous (see Fig. 3b).

Analytical photography

Analytical photography is a tool that enables capturing a faithful representation of an object and revealing information that remains invisible to the naked eye. Visualising the structures and subtle differences in the material composition fosters better understanding of the object's history, technology used to create it, and the changes that have affected it over time.

The Vis-band photograph included below shows the general state of preservation of the work. The IR photograph reveals fragments of the hidden compositions – a portrait and a horse-rider (marked in yellow in Fig. 4b). The UV image shows the locations of secondary layers and conservation work carried out to date.

Visible-light photography is primarily used for documenting the current state of conservation. By reconfiguring the geometry of the measurement process, it is also possible to capture images of objects with side lightning and with light shining through them (examples in Fig. 5). These photographs contain information about possible irregularities in the object's surface, the application of the paint layers and the thickness of the layers.

Due to the reduced ability of longer-wavelength waves (including infrared spectrum) to interact with matter, infrared reflectography provides information about the drawings, sketches and compositional changes of the analysed works (Figs 4b and 6).

Many organic compounds exhibit significant UV light absorption, which results in the emission of radiation in the visible wavelength range.

Fig. 4a–c

Photographs in various electromagnetic radiation bands presenting the painting *A Study of a Bearded Peasant* by Piotr Michałowski, held by the National Museum in Cracow. Reflected light (a) Vis, (b) IR, (c) UV-induced Vis

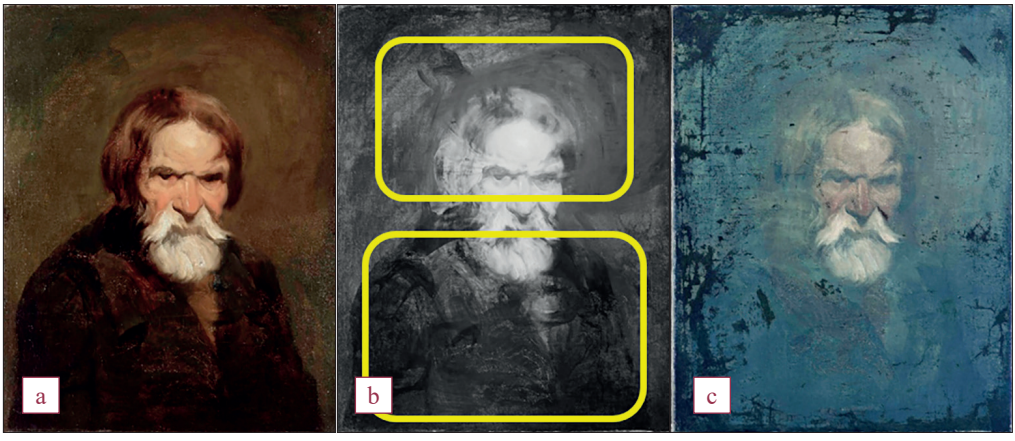

Fig. 5a–b

The painting *A Group of Saints* by Bernardo Daddi, held by the National Museum in Cracow: (a) visible light photography in reflected and laterally reflected light; (b) reverse of a painting captured with light shining through

Thanks to this phenomenon, many substances of organic and non-organic origin, such as natural and artificial resins, can be seen and identified on the basis of UV-induced photographs (Figs 4c and 7).[17] For example, the characteristic orange fluorescence (indicated by yellow arrows in Fig. 7) in the green sections indicates that the artist used cadmium yellow.

The response to UV light irradiation for some materials changes over time – this property can be used as a way to date the painting.[18] This phenomenon is also used for discovering secondary layers. For example, old varnish emits different wavelengths when compared to freshly applied varnish in the areas where conservation work was carried out.

17 E. Rene de la Rie, 'Fluorescence of Paint and Varnish Layers (Part I)', *Studies in Conservation*, vol. 27, 1982, pp. 1–7.

18 M. Thoury et al., 'Nondestructive Varnish Identification by Ultraviolet Fluorescence Spectroscopy', *Applied Spectroscopy*, vol. 61(12), 2007.

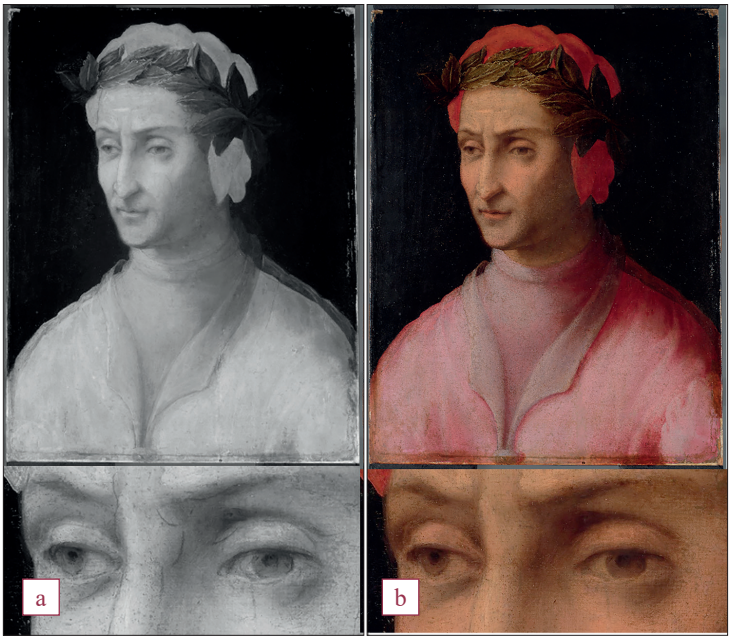

Fig. 6a–b

The painting *A Portrait of Dante* by an anonymous painter, held by the National Museum in Cracow, top – the entire painting, below – selected detail; (a) IR reflectogram, (b) photograph in visible light; the IR photograph reveals the drawing and the extent of the author's change to the outline of the figure

Fig. 7a–b

The painting *A Forest Road* by Józef Chełmoński, held by the National Museum in Cracow: painting in visible light and in UV-induced visible light

Hyperspectral imaging

Radiometric calibration and obtaining a spectrum

The intensity for each pixel in the resulting hyperspectral (and multispectral) images are represented by numerical values (DN – digit numbers or DC – digital counts), which represent a signal proportional to the change in current in the sensor's circuit resulting from the registration of a quantum of light. The DN values correspond to the reflectance level of the surface and include information about the characteristics of the sensor used (gain and offset), as well as irregular lighting. To compensate for these factors, DN is converted to reflectance values in a process called radiometric calibration.[19] This process involves several steps,

19 J. Dyer, G. Verri, J. Cupitt, *Multispectral Imaging*; R. Pillay, J. Y. Hardeberg, S. George, 'Hyperspectral Calibration of Art'; Jones et al., 'Understanding Multispectral Imaging'; D. D. R. Kohler et al., 'New approach for the radiometric calibration of spectral imaging systems', *Optics Express*, vol. 12(11), 2007, pp. 2463–2477; M. S. Shaikh et al.,

including the dark current and flat-field corrections mentioned earlier, as well as spectral calibration.

The latter leads to the determination of the reflectance $\rho(\lambda)$, which is defined as the ratio of the light reflected from the imaged surface to the light cast on that surface:

$$\rho(\lambda)_t = \frac{\phi_{r,t}(\lambda)}{\phi_{i,t}(\lambda)}$$

where: $\rho(\lambda)_t$ – reflectance of a given point of the object (t – 'target'), in dimensionless quantities, with a value in the range of [0-1],
$\phi_{r,t}(\lambda)$ – the ligt reflected from the target (r – 'reflected') of the imaged surface
$\phi_{i,t}(\lambda)$ – the light incident on the target (i – 'incident') of the imaged surface.

In laboratory conditions, calibration is carried out using artificial lighting based on Lambertian reflectance[20] standards (e.g. Spectralon targets[21]) with known reflectance in a given EM spectral range.

The formula below describes the value (pixel intensity, or DN) captured by the sensor as a result of the measurement:

$$DN_\lambda = g\phi_r(\lambda) + b$$

where DN_λ – pixel brightness value for the spectral channel corresponding to λ,
g – coefficient corresponding to the sensor gain and accumulation time,
b – offset, the base value of the dark current.

In the case of the target, it can be expressed as

$$\rho_r = \frac{\phi_{r,r}}{\phi_{i,r}} = \frac{x}{100}$$

where ρ_r – target reflectance, r from reference,
$\phi_{r,r}$ – light reflected from the target,
$\phi_{i,r}$ – light incident on the target,
x – the percentage of target reflectance guaranteed by the manufacturer.

'Calibration of a Hyper-Spectral Imaging System Using a Low Cost Reference', *Sensors* (Basel), vol. 21(11), 2021.

20 J. H. Lambert, *Photometrie. Photometria sive de mensural de gradibus luminis, colorum et umbrae*, Augsburg, 1760; S. J. Koppal, 'Lambertian Reflectance', in: *Computer Vision*, ed. K. Ikeuchi, 2014, pp. 441–443.

21 labsphere.com/product/spectralon-reflectance-targets/ (accessed 20 May 2024).

When the target is characterised by maximum reflectance, then

$$\phi_{r,r} = \phi_{i,r}$$

Bearing in mind that the measurements of the target and the object are carried out in the same conditions, it can be assumed that $\phi_{i,t}(\lambda) = \phi_{i,r}(\lambda)$. Thus, in order to obtain the reflectance of the object, a divide-by-target operation needs to be performed and the dark current image needs to be subtracted from both the target image and the captured target:

$$\rho(\lambda)_t = \frac{g\phi_{r,t}(\lambda) - b}{g\phi_{r,r}(\lambda) - b} = \frac{DN_{\lambda,t} - b}{DN_{\lambda,r} - b}$$

It can be easily seen that in the case of hyperspectral images, the above operation includes not only spectral calibration, but also flat-field and dark current correction.

Ways of presenting hyperspectral data

The visualisation of multidimensional data, including hyperspectral images, is a challenging task, as it generally requires performing an appropriate interpretation of the data in line with the aim of the study.

One of the more popular ways of visualising hyperspectral data is to present them as material distribution maps. There are a number of different strategies for developing such maps. If the material make-up of the object is unknown, certain endmembers need to be identified to represent as many of the materials that make up the object as possible. The PPI (Pixel Purity Index[22]) algorithm can be used to aid that, as well as a number of algorithms that reduce the dimensionality of data, such as factorisation algorithms (including PCA – Principal Component Analysis[23] and others[24]) as well as the t-SNE (t-Distributed Stochastic Neighbour Embedding[25]) method or the UMAP (Uniform Manifold Approximation and Projection for Dimension Reduction[26])

22 C.-I. Chang, A. Plaza, 'A Fast Iterative Algorithm For Implementation of Pixel Purity Index', *IEEE Geoscience and Remote Sensing Letters*, vol. 3(1), 2006, pp. 63–67.

23 J. Sandak et al., 'Nondestructive Evaluation of Heritage Object Coatings with Four Hyperspectral Imaging Systems', *Coatings*, vol. 11(2), 2021.

24 B. Łach et al., 'Application of Factorisation Methods to Analysis of Elemental Distribution Maps Acquired with a Full-Field XRF Imaging Spectrometer', *Sensors*, vol. 21, 2021.

25 M. Alfeld, 'Joint data treatment for Vis-NIR reflectance imaging spectroscopy and XRF imaging acquired in the Theban Necropolis in Egypt by data fusion and t-SNE', *Comptes Rendus Physique*, vol. 19(7), 2018, pp. 625–635.

26 M. Vermeulen et al., 'Application of Uniform Manifold Approximation and Projection (UMAP) in spectral imaging of artworks', *Spectrochimica Acta Part A: Molecular and Biomolecular Spectroscopy*, vol. 252, 2021.

algorithm. Areas with high PPI, which are of interest to the researcher, can also be picked manually by selecting the ROI (Region of Interest).

Once the spectra of components within the work have been obtained, an attempt can be made to develop distribution maps. For this purpose, the SAM (Spectral Angle Mapper[27]) can be used according to the following formula:

$$\alpha = cos^{-1}\left(\frac{\sum_{i=1}^{n} t_i r_i}{\sqrt{\sum_{i=1}^{n} t_i^2}\sqrt{\sum_{i=1}^{n} r_i^2}}\right)$$

where α – spectral similarity coefficient, the SAM spectral angle takes values of $[0–\frac{\pi}{2}]$, with 0 indicating identical spectra;

t_i – intensity for the i[th] band in the spectrum of a given point of the object (t – from *target*),

r_i – intensity for the i[th] band in the reference spectrum (one of the component spectra);

n – number of spectral bands.

When using SAM, the classification threshold – the value for which the analysed spectrum can be classified as the same as the reference spectrum – needs to be carefully selected. An example of spectral angle mapping is shown in Fig. 8.

Material distribution maps can also be obtained using other measures of spectral similarity, including SCM (Spectral Correlation Mapper[28]) and the KLPD (Kullback-Leiber Pseudo Divergence[29]).

The use of dimensionality-reducing algorithms, such as the aforementioned factorisation methods, can also result in obtaining material distribution data as a result of an algorithmic transformation (factor scores and shape analysis of the resulting factors[30]). Clustering of the t-SNE-reduced data could also leads to obtaining material distribution maps.[31]

If possible, the material distribution of the piece can also be obtained by calculating the integrals of material-specific spectral structures

27 Jones et al., 'Understanding Multispectral Imaging', pp. 339–350.

28 B. M. Devassy et al., 'Classification of forensic hyperspectral paper data using hybrid spectral similarity algorithms', *Journal of Chemometrics*, vol. 36(1), 2022.

29 N. Richard et al., 'Pseudo-Divergence and Bidimensional Histogram of Spectral Differences for Hyperspectral Image Processing', *Journal of Imaging Science and Technology*, vol. 60(5), 2016.

30 Łach et al., 'Application of Factorisation Methods'.

31 Alfeld, 'Joint data treatment'.

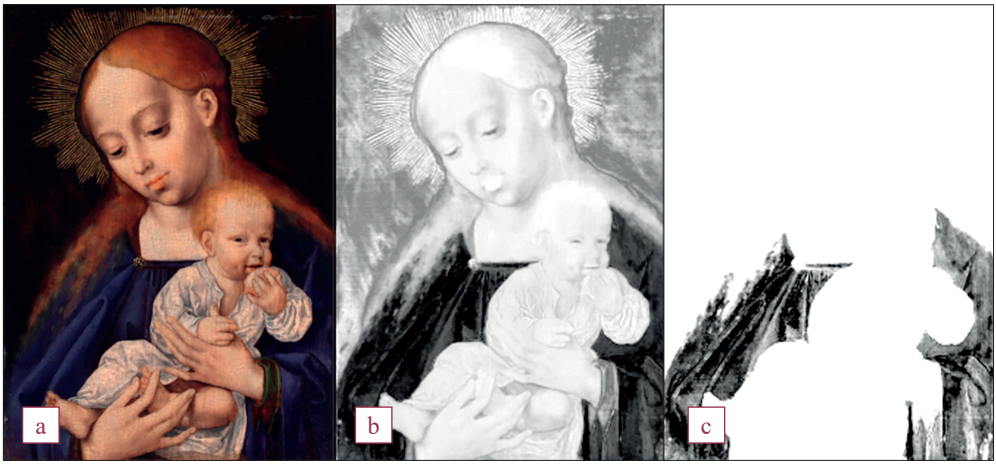

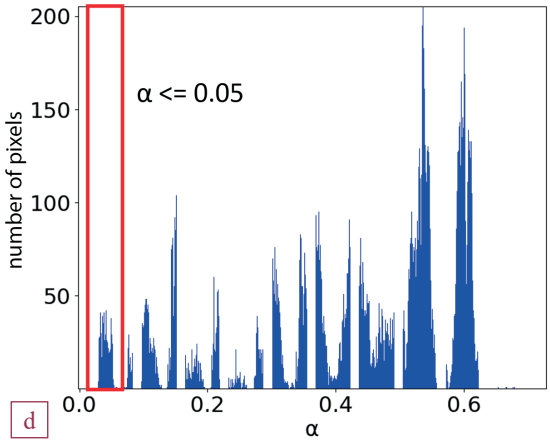

Fig. 8a–d

Fig. 8. SAM spectral angle mapping: (a) painting in visible light (*Virgin Mary with the Child Jesus Eating an Apple* by Joos van Cleve, held by the National Museum in Cracow), (b) map of SAM values, (c) map of SAM values with the 0.05 threshold – azurite distribution, (d) histogram of SAM values within the image. Based on the shape, the values of the classification threshold can be iteratively chosen. In the case in question, the extreme values (á) are equal to 0.023 and 0.7

in the spectrum.[32] However, it is important to bear in mind that a high heterogeneity of the object's make-up has an impact on the complex shapes of its spectra: many bands can interfere and distort the final calculation result.

Where a database of reference spectra is available, it is advisable to consider applying Deep Learning algorithms and neural networks to carry out this work.[33] Studies focusing on the application of deep learning and neural network for material identification and material distribution mapping in the analysis of works of art have picked up pace in recent years.[34]

32 F. Gabrieli et al., 'Near-UV to mid-IR reflectance imaging spectroscopy of paintings on the macroscale', *Science Advances*, vol. 5(8), 2019.

33 E. Pouyet et al., 'Artificial Intelligence for Pigment Classification Task in the Short-Wave Infrared Range', *Sensors*, vol. 21(8), 2021. T. Kleynhans et al., 'An alternative approach to mapping pigments in paintings with hyperspectral reflectance image cubes using artificial intelligence', *Heritage Science*, vol. 8(84), 2020.

34 Picollo et al., 'Hyper-Spectral Imaging Technique'; L. Liu, E. Pouyet et al., 'Neural Networks for Hyperspectral Imaging of Historical Paintings. A Practical View', *Sensors*, vol. 23(5), 2023.

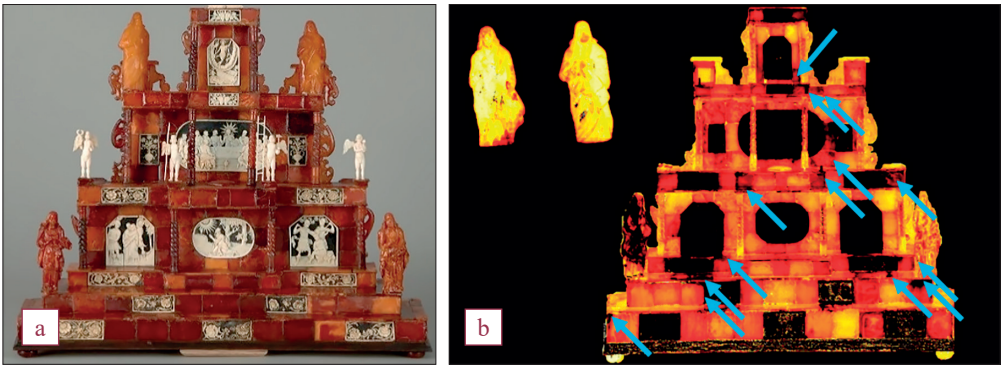

Fig. 9a–b

The Altar of the Passion of Christ by Michael Schödelock, held by the National Museum in Cracow: (a) visible-light photograph of the analysed object; (b) map indicating faux amber locations obtained using the Golloch formula, with common parts – I_1 and I_2

In some cases, the nature of the object requires using different solutions for presenting the required data. In these cases, one should approach the process on a case-by-case basis following a thorough analysis of the multispectral data. The example above (Fig. 9) shows an image with the locations of cavities in the amber plaques of *The Altar of the Passion of Christ* (National Museum in Cracow), obtained thanks to spectral analysis. To determine the sites where an imitation of amber was used, the formula proposed by A. Golloch was used[35]:

$$I_{1,2} = \frac{x_{1,2} - a}{b - a}$$

where $x_{1,2}$ – reflectance intensity at 1415 and 1555 nm, respectively;
a – reflectance intensity at 1200 nm;
b – reflectance intensity at 1315 nm.

The spectrum of amber shows a characteristic pattern with a series of local absorption maxima for 1200, 1415 and 1639 nm and maximum reflectance for 1115, 1315, 1555, 1654 nm. Selected wavelengths are highlighted in the formula above. Based on the shape of the spectrum and the intensity of the highlighted bands, amber can be differentiated from many other resins.

The locations of cavities filled with synthetic resin are identified by the values of the I coefficients in the Golloch formula, which are different from those indicating amber (additional reference analyses and comparison with existing data sources are necessary for this purpose). In Figure 9b, the orange shades indicate the locations where amber was found; the black colour represents other materials, which can be found within the amber altar and the background (the I values do not correspond to amber reference values). Parts of the amber plaques are dark; this means that the existing cavities were probably filled with amber imitation material (examples of this are marked with arrows in Fig. 9b).

35 A. Golloch, S. Heidbreder, C. Luhr, 'Identification of amber and imitations by near infrared reflection spectroscopy', *Fresenius' Journal of Analytical Chemistry*, vol. 361, 1998, pp. 545–546.

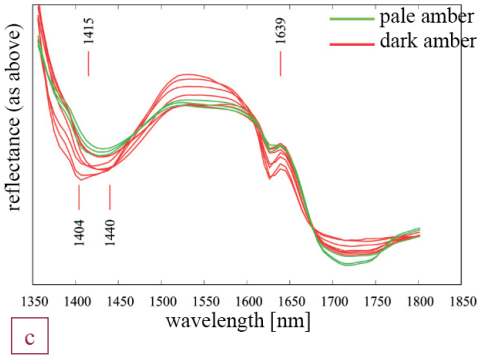

Fig. 10a–c

The Altar of the Passion of Christ by Michael Schödelock, held by the National Museum in Cracow: (a) and (b) FC images of an amber altarpiece; (a) FC bands (1515, 1404, 1639 nm) selected based on changes in (c) the spectra of the two classes of amber that make up the object

Another popular method for presenting hyperspectral data is the false colours method. To use it, one needs to select three captured images to be assigned to RGB channels. The selection should not be random, but based on the spectral characteristics of the data presented. There are attempts to standardise this method of visualising hyperspectral images;[36] however, it remains a challenge due to the high complexity of the analysed objects. An example of an FC visualisation is shown in Fig. 10.

Originally, the amber plaques were made of pale and dark amber arranged in an alternating pattern, which is no longer visible (in visible-light photographs, see Fig. 9a, and FC images with randomly selected RGB channels, see Fig. 10b). However, these differences remain clear when the spectra are concerned – pale types of amber are characterised by less intense bands (attributed to the presence of succinic acid) because they have relatively more air inclusions in their structure.[37]

The analysis strategies and the methods of developing visualisations should be chosen after a comprehensive description including the

36 A. Cosentino, 'Effects of different binders on technical photography and infrared reflectography of 54 historical pigments', *International Journal of Conservation Science*, vol. 6(3), 2015, pp. 287–298.

37 P. Krupska-Wolas et al., 'SWIR Reflectance Imaging Spectroscopy and Raman Spectroscopy Applied to the Investigation of Amber Heritage Objects. Case Study on the Amber Altar of the Lord's Passion', in: *The Future of Heritage Science and Technologies* (Lecture Notes in Mechanical Engineering), ed. R. Furferi et al., 2023.

rationale for the choice, which would enable the process to be repeated in the future. This could enable carrying out a comparative analysis, should such a need arise.

Conclusions

Broad-spectrum EM imaging is a valuable tool that enables obtaining faithful reproductions of objects, as well as looking deeper in order to discover layers invisible to the naked eye, to assess these objects' material composition, manufacturing technology, age, and changes that have occurred in them over time, whether due to human intervention or degradation.

The difference between multiband imaging and multispectral/hyperspectral imaging lies in the calibration of the images against a reflectance target, which allows spectral information to be obtained from every point in the image.

With radiometric calibration, the PPI values in the image reflect the physical and chemical material characteristics of the analysed object (reflectance) while the impact of the devices and irregular lighting is compensated for.

Collecting spectral data enables carrying out a sophisticated analysis of various information in order to search for the answer to a variety of research questions. The methods used for visualising the data in question thus require appropriate interpretation, which can be challenging due to the need to understand hyperspectral image analysis methods. It is also worth noting that establishing a universal strategy for visualising the data remains a key challenge, since it strictly depends on the analysed object, its composition and structure.

In order to obtain maps of the material distribution of the analysed object, one needs to have reference spectra (either internal, obtained directly from the object, or external), which can be then compared with each spectrum of the analysed image using the SAM technique. There are many methods of obtaining spectral data of the endmembers of an analysed object – ROI, PPI, factorisation methods, t-SNE and others. In recent years, solutions based on deep learning algorithms have also gained popularity.

The issue of making hidden layers visible, together with material identification, requires a customised analysis adapted to the spectral characteristics of the object.

It is also important to prepare a comprehensive description of the data analysis strategy, which includes an explanation of the rationale for choosing specific algorithms, thus enabling the process to be repeated should the need arise in the future.

BIBLIOGRAPHY

Abdlaty R., Fang Q., 'Acousto-optic tunable filter-based hyperspectral imaging system characterization, SPIE BiOS 2019', *Design and Quality for Biomedical Technologies XII*, 2019.

Alfeld M., 'Joint data treatment for Vis-NIR reflectance imaging spectroscopy and XRF imaging acquired in the Theban Necropolis in Egypt by data fusion and t-SNE', *Comptes Rendus Physique*, vol. 19(7), 2018, pp. 625–635.

Alfeld M. et al., 'A mobile instrument for in situ scanning macro-XRF investigation of historical paintings', *Journal of Analytical Atomic Spectrometry*, vol. 28(5), 2013, pp. 760–767.

Catelli E. et al., 'Towards the non-destructive analysis of multilayered samples: A novel XRF-VNIR-SWIR hyperspectral imaging system combined with multiblock data processing', *Analytica Chimica Acta*, vol. 1239, 2023, pp. 1–9.

Chang C.-I., Plaza A., 'A Fast Iterative Algorithm For Implementation of Pixel Purity Index', *IEEE Geoscience and Remote Sensing Letters*, vol. 3(1), 2006, pp. 63–67.

Cosentino A., 'Effects of different binders on technical photography and infrared reflectography of 54 historical pigments', *International Journal of Conservation Science*, vol. 6(3), 2015, pp. 287–298.

Delaney J. K. et al., 'Visible and infrared imaging spectroscopy of paintings and improved reflectography', *Heritage Science*, vol. 4(6), 2016, pp. 1–10.

Delaney J. K. et al., 'Integrated X-ray fluorescence and diffuse visible-to-near-infrared reflectance scanner for standoff elemental and molecular spectroscopic imaging of paints and works on paper', *Heritage Science*, vol. 6(31), 2018, pp. 1–12.

Devassy B. M. et al., 'Classification of forensic hyperspectral paper data using hybrid spectral similarity algorithms', *Journal of Chemometrics*, vol. 36(1), 2022, pp. 1–13.

Dyer J., Verri G., Cupitt J., *Multispectral Imaging in Reflectance and Photo-induced Luminescence modes. A User Manual*, 2013, researchgate.net/publication/267266175_Multispectral_Imaging_in_Reflectance_and_Photo-induced_Luminescence_modes_A_User_Manual (accessed 20 May 2024).

Gonzales V. et al., 'X-ray Diffraction Mapping for Cultural Heritage Science: a Review of Experimental Configurations and Applications', *Chemistry. A European Journal*, vol. 26(8), 2020, pp. 1703–1719.

Gabrieli F. et al., 'Near-UV to mid-IR reflectance imaging spectroscopy of paintings on the macroscale', *Science Advances*, vol. 5(8), 2019, pp. 1–10.

Golloch A., Heidbreder S., Luhr C., 'Identification of amber and imitations by near infrared reflection spectroscopy', *Fresenius' Journal of Analytical Chemistry*, vol. 361, 1998, pp. 545–546.

Hagen N. et al., 'Snapshot advantage. A review of the light collection improvement for parallel high-dimensional measurement systems', *Optical Engineering*, vol. 51, 2012, pp. 1–7.

Hoek C. J. G. van et al., 'A SEM-EDS Study of Cultural Heritage Objects with Interpretation of Constituents and Their Distribution Using PARC Data Analysis', *Microscopy and Microanalysis*, vol. 17(5), 2011, pp. 656–660.

Jablonski A., 'Efficiency of Anti-Stokes Fluorescence in Dyes', *Nature*, vol. 131, 1933, pp. 839–840.

Jones C. et al., 'Understanding Multispectral Imaging of Cultural Heritage. Determining Best Practice in MSI Analysis of Historical Artefacts', *Journal of Cultural Heritage*, vol. 45, 2020, pp. 339–350.

Kleynhans T. et al., 'An alternative approach to mapping pigments in paintings with hyperspectral reflectance image cubes using artificial intelligence', *Heritage Science*, vol. 8(84), 2020, pp. 1–16.

Kohler D. D. R. et al., 'New approach for the radiometric calibration of spectral imaging systems', *Optics Express*, vol. 12(11), 2007, pp. 2463–2477.

Koppal S. J., 'Lambertian Reflectance', in: *Computer Vision*, ed. K. Ikeuchi, 2014, pp. 441–443.

Krupska-Wolas P. et al., 'SWIR Reflectance Imaging Spectroscopy and Raman Spectroscopy Applied to the Investigation of Amber Heritage Objects. Case Study on the Amber Altar of the Lord's Passion', in: *The Future of Heritage Science and Technologies* (Lecture Notes in Mechanical Engineering), ed. R. Furferi et al., 2023, pp. 401–419.

Lakowicz J. R., *Principles of Fluorescence Spectroscopy*. *Third edition*, 2006.

Lambert J. H., *Photometrie. Photometria sive de mensural de gradibus luminis, colorum et umbrae* (Augsburg, 1760).

Lee H., Kim M. H., 'Building a Two-Way Hyperspectral Imaging System with Liquid Crystal Tunable Filters', in: *Image and Signal Processing, 6th International Conference, ICISP 2014* (Lecture Notes in Computer Science), vol. 8509, 2014.

Lee H., *Introduction to Color Imaging Science* (New York, 2005).

Liu L., Pouyet E. et al., 'Neural Networks for Hyperspectral Imaging of Historical Paintings. A Practical View', *Sensors*, vol. 23(5), 2023, pp. 1–25.

Łach B. et al., 'Application of Factorisation Methods to Analysis of Elemental Distribution Maps Acquired with a Full-Field XRF Imaging Spectrometer', *Sensors*, vol. 21, 2021, pp. 1–19.

Picollo M. et al., 'Hyper-Spectral Imaging Technique in the Cultural Heritage Field. New Possible Scenarios', *Sensors*, vol. 20(10), 2020, pp. 1–12.

Pillay R., Hardeberg J.Y., George S., 'Hyperspectral Calibration of Art: Acquisition and Calibration Workflows', *Journal of the American Institute of Conservation*, vol. 58(1), 2019, pp. 1–10.

Pouyet E. et al., 'Artificial Intelligence for Pigment Classification Task in the Short-Wave Infrared Range', *Sensors*, vol. 21(8), 2021, pp. 1–11.

Pust O., 'Innovative Filter Solutions for Hyperspectral Imaging', *Optik & Photonik*, vol. 11(3), 2016, pp. 1–4.

Rene de la Rie E., 'Fluorescence of Paint and Varnish Layers (Part I)', *Studies in Conservation*, vol. 27, 1982, pp. 1–7.

Richard N. et al., 'Pseudo-Divergence and Bidimensional Histogram of Spectral Differences for Hyperspectral Image Processing', *Journal of Imaging Science and Technology*, vol. 60(5), 2016, pp. 1–13.

Rousaki A., Vandenabeele P., 'In situ Raman spectroscopy for cultural heritage studies', *Journal of Raman Spectroscopy*, vol. 52, 2021, pp. 2178–2189.

Sandak J. et al., 'Nondestructive Evaluation of Heritage Object Coatings with Four Hyperspectral Imaging Systems', *Coatings*, vol. 11(2), 2021, pp. 1–15.

Shaikh M. S. et al., 'Calibration of a Hyper-Spectral Imaging System Using a Low Cost Reference', *Sensors* (Basel), vol. 21(11), 2021, pp. 1–19.

Smieska L. M. et al., 'Synchrotron-Based High-Energy X-ray MA-XRF and MA-XRD for Art and Archaeology', *Synchrotron Radiation News*, vol. 32(6), 2019, pp. 29–33.

Striova J. et al., 'Reflectance imaging spectroscopy in heritage science', *La Rivista del Nuovo Cimento*, vol. 43, 2020, pp. 515–566.

Technical Report. Colorimetry, International Commission on Illumination, 2004, cielab.xyz/pdf/cie.15.2004%20colorimetry.pdf (accessed 20 May 2024).

Thoury M. et al., 'Nondestructive Varnish Identification by Ultraviolet Fluorescence Spectroscopy', *Applied Spectroscopy*, vol. 61(12), 2007, pp. 1–8.

Vermeulen M. et al., 'Application of Uniform Manifold Approximation and Projection (UMAP) in spectral imaging of artworks', *Spectrochimica Acta Part A: Molecular and Biomolecular Spectroscopy*, vol. 252, 2021, labsphere.com/product/spectralon-reflectance-targets/ (accessed 20 May 2024).

LIST OF ILLUSTRATIONS

p. 225 Diagram of a test bed for multiband and multispectral imaging in the reflection mode. The light source should be angled at 45° to avoid specular reflections from the object. Depending on the lighting used and the desired resulting image, the positioning and type of band-pass filters used (indicated by blue arrows) can be freely modified. Filters in the object-to-camera path can also be replaced by a suitable optical system equipped with dispersive elements and readout electronics adapted to this kind of process; fig. by Paulina Krupska-Wolas

p. 227 A selected frame from the painting *A Portrait of Dante* by an anonymous painter, held by the National Museum in Cracow (inv. no. MNK XII-218): (a) fragment of the raw image without pre-processing; (b) dark current image; (c) white field image; (d) resulting processed image. In the case of images in the visible light spectrum, an additional correction against a colour test target (e.g. ColorChecker) needs to be carried out to ensure proper colour reproduction; fig. by Paulina Krupska-Wolas

p. 228 Conceptual representation of (a) multiband and (b) multispectral images; fig. by Paulina Krupska-Wolas

p. 229 Photographs in various electromagnetic radiation bands presenting the painting *A Study of a Bearded Peasant* by Piotr Michałowski, held by the National Museum in Cracow (inv. no. MNK II-a-728), photo by Michał

Obarzanowski and Piotr Frączek; fig. by Paulina Krupska-Wolas based on photographic documentation by M. Obarzanowski and P. Frączek

p. 230 The painting *A Group of Saints* by Bernardo Daddi, held by the National Museum in Cracow (inv. no. MNK XII-180); photo by Michał Obarzanowski and Tomasz Wilkosz

p. 231 The painting *A Portrait of Dante* by an anonymous painter, held by the National Museum in Cracow (inv. no. MNK XII-218): op – the entire painting, below – selected detail; (a) IR reflectogram, (b) photograph in visible light; photo by Michał Obarzanowski and Tomasz Wilkosz

p. 231 The painting *A Forest Road* by Józef Chełmoński, held by the National Museum in Cracow (inv. no. MNK II-a-432); photo by Michał Obarzanowski and Tomasz Wilkosz

p. 235 SAM spectral angle mapping: (a) The painting in visible light (*Virgin Mary with the Child Jesus Eating an Apple* by Joos van Cleve, held by the National Museum in Cracow, inv. no. MNK XII-255), (b) map of SAM values, (c) map of SAM values with the 0.05 threshold – azurite distribution, (d) histogram of SAM values within the image; fig. by Paulina Krupska-Wolas based on photographs by Michał Obarzanowski and Tomasz Wilkosz

p. 236 *The Altar of the Passion of Christ* by Michael Schödelock, held by the National Museum in Cracow (inv. no. MNK XIII-446): (a) visible-light photograph of the analysed object – Michał Obarzanowski and Piotr Frączek; (b) map indicating faux amber locations obtained using the Golloch formula; fig. by Paulina Krupska-Wolas based on photographs by Michał Obarzanowski and P. Frączek

p. 237 *The Altar of the Passion of Christ* by Michael Schödelock, held by the National Museum in Cracow (inv. no. MNK XIII-446); fig. by Paulina Krupska-Wolas

PAULINA KRUPSKA-WOLAS
https://orcid.org/0000-0001-8276-380X

She has begun her doctoral studies in 2021. Her dissertation focuses on the use of neural networks for material identification in historic objects using VNIR/SWIR reflectance spectroscopy (RIS) and XRF macrospectroscopy (MA-XRF) imaging. She graduated from the Faculty of Physics and Applied Computer Science at the AGH University of Science and Technology, with a major in imaging techniques and biometrics. Since 2018, she has been working with the Laboratory of Analysis and Nondestructive Investigation of Heritage Objects of the National Museum in Cracow, analysing artefacts using the RIS and MA-XRF techniques to deepen the understanding of the materials and techniques used. She performs multivariate data analysis and applies advanced statistical methods to both imaging and point spectroscopy data.

The study was conducted as part of the statutory work of the National Museum in Cracow.

Contact: pkrupska@mnk.pl

MICHAŁ OBARZANOWSKI
https://orcid.org/0000-0001-9150-2724

A graduate of the Faculty of Conservation and Restoration of Works of Art at the Academy of Fine Arts in Cracow. He is a senior art conservator at the National Museum in Cracow, where he is responsible for the conservation of objects in the collections of the Museum, with particular focus on the full range of both traditional and atypical materials. Member of the research and conservation teams involved with the analyses and studies of Hans Memling's *The Last Judgement*, El Greco's *The Ecstasy of St Francis* and Vincent van Gogh's *Cottages among Trees*. Designer and builder of microclimatic frames used by many Polish museums. Since 2004, he has been involved in the work of the Laboratory of Analysis and Nondestructive Investigation of Heritage Objects at the National Museum in Cracow, where he focuses on analytical photography, digital x-ray imaging, as well as running and participating in the projects under the auspices of the National Heritage Research Centre. Author and co-author of several published studies, as well as numerous conference papers.

The study was conducted as part of the statutory work of the National Museum in Cracow.

Contact: mobarzanowski@mnk.pl

TOMASZ WILKOSZ
https://orcid.org/0000-0002-8192-8788

Holding a doctorate in chemistry from the Jagiellonian University is a specialist combining scientific knowledge with practical industrial applications. Throughout his career, he coordinated and supervised research and development projects which resulted in patents in the field of environmental catalysis. Since 2019, he has been working as an expert for analytical photography and X-ray imaging at the National Museum in Cracow, where he is involved in advanced analyses of works of art and the preparation of expert reports concerning cultural heritage.

The study was conducted as part of the statutory work of the National Museum in Cracow.

Contact: twilkosz@mnk.pl

JULIO M. DEL HOYO-MELÉNDEZ
https://orcid.org/0000-0003-2163-2149

Graduated with a Master's degree in chemistry from the University of Houston in the United States and successfully defended his PhD dissertation at the Technical University of Valencia (Spain) in 2010. Since 2011, he has been working at the Laboratory of Analysis and Nondestructive Investigation of Heritage Objects at the National Museum in Cracow, of which he has been the head since 2017, along with the National Heritage Research Centre. He has been editor-in-chief of the *Journal of the American Institute for Conservation* since 2014.

The study was conducted as part of the statutory work of the National Museum in Cracow.

Contact: jdelhoyo@mnk.pl